

**Exact Solutions for Wind-Driven Coastal Upwelling and Downwelling over Sloping
Bathymetry**

DANA LYNN DUKE AND PAUL DEREK SINZ

Mathematics Department
California Polytechnic State University
San Luis Obispo, California
June 2010
© 2010 Dana Duke and Paul Sinz

ABSTRACT

The dynamics of wind-driven coastal upwelling and downwelling are studied using a simplified dynamical model. Exact solutions are examined as a function of time and over a family of sloping bathymetries. Assumptions in the two-dimensional model include a frictionless ocean interior below the surface Ekman layer, and no alongshore dependence of the variables; however, dependence in the cross-shore and vertical directions is retained. Additionally, density and alongshore momentum are advected by the cross-shore velocity in order to maintain thermal wind. The time-dependent initial-value problem is solved with constant initial stratification and no initial alongshore flow. An alongshore pressure gradient is added to allow the cross-shore flow to be geostrophically balanced far from shore. Previously, this model has been used to study upwelling over flat-bottom and sloping bathymetry, but the novel feature in this work is the discovery of exact solutions for downwelling. These exact solutions are compared to numerical solutions from a primitive-equation ocean model, based on the Princeton Ocean Model, configured in a similar two-dimensional geometry. Many typical features of the evolution of density and velocity during downwelling are displayed by the analytical model.

ACKNOWLEDGEMENTS

We would like to thank Professor Paul Choboter for creating this research project and for his guidance throughout the process. Also, thanks to JP Horton for his unwavering support, Maple skills, and large contributions to this research. This project could not have been completed without the aid of both. May they live long and prosper.

CONTENTS

List of Figures	4
I. Introduction	5
II. Assumptions	5
III. Thermal Wind	7
IV. Solutions	10
V. The Stream Function	12
VI. Summary of Work	13
VII. Algebraic Methods	13
VIII. Notable Features	14
IX. Comparison to a Numerical Model	17
X. Concluding Remarks	18
Appendix A. The Zero-Contour of $v(x, z, t)$	19
Appendix B. The Front of the Mixed Region	22
Appendix C. Substituting the Solutions into the Transformed Differential Equations	23
References	26

LIST OF FIGURES

1	Schematics illustrating the key assumptions in model of upwelling and downwelling.	5
2	Satellite image of North America showing chlorophyll concentrations, indicative of coastal upwelling.	6
3	Hydrostatic balance is illustrated.	8
4	Geostrophic balance and thermal wind are illustrated.	8
5	Illustration of the Coriolis force.	9
6	A characteristic plot of downwelling, modeled by the analytic function.	12
7	The stream functions for upwelling and downwelling compared.	13
8	The time progression of bottom bathymetry.	15
9	Downwelling over various bottom bathymetries after approximately six days.	16
10	A characteristic plot of downwelling for POM2D.	18
11	Time progressions (10 days, 16 days, and 23 days) are shown here comparing density and along slope velocity between the analytical and numerical models.	19

I. INTRODUCTION

The prevailing winds off the California coast blow predominately southward during the summer months. Due to the Coriolis force, the water along the surface of the ocean turns to its right, away from shore. This net offshore displacement causes deeper water to swell upward and replace the coastal surface layer in a phenomenon known as upwelling. The process of upwelling brings vital nutrients from the ocean floor to coastal ecosystems. These nutrients consist of decaying plant and animal materials that are drawn up with the fluid to higher depths inhabited by most sea life. The satellite image in Figure 2 shows the connection between upwelling and its ecological impact. Upwelling is also responsible for the cool, foggy weather in summertime. Water from the depths is cold and dense. When that water meets the warm summer air at the surface, it condenses, creating fog.

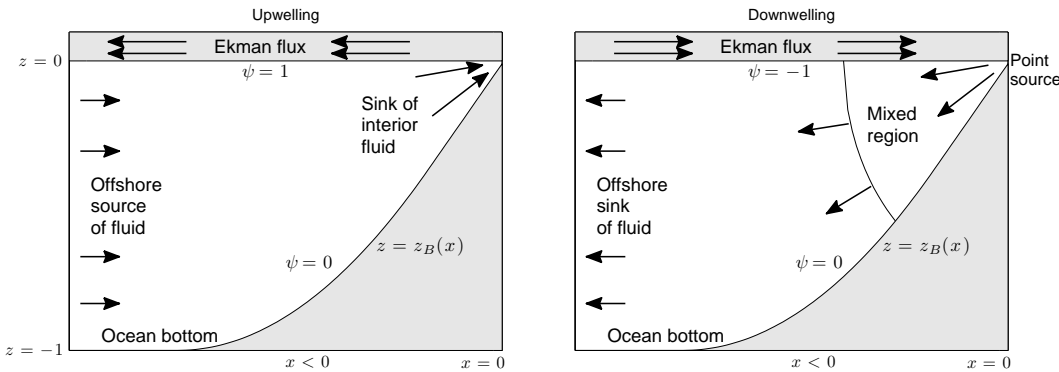


FIGURE 1. Schematics illustrating the key assumptions in model of upwelling and downwelling. The gray area represents bottom bathymetry. Fluid flow is indicated by the black arrows. These schematics include the turbulent Ekman layer.

Its counterpart, downwelling, occurs when the wind blows northward, forcing the top layer of the ocean towards the shoreline. This causes the water beneath the surface layer to be pushed offshore. It typically occurs during winter storms. Upwelling occurs throughout the summer for months at a time. Compared to downwelling, it is a long term phenomenon. Downwelling events occur on the order of days. In real life, there is usually some combination of upwelling and downwelling in various stages at any given time. The model we will discuss treats upwelling and downwelling as separate cases. See Figure 1.

II. ASSUMPTIONS

Although the ocean is a complex system, we can model the fluid dynamics of upwelling and downwelling with exact mathematical equations if we make appropriate assumptions. The following nondimensional

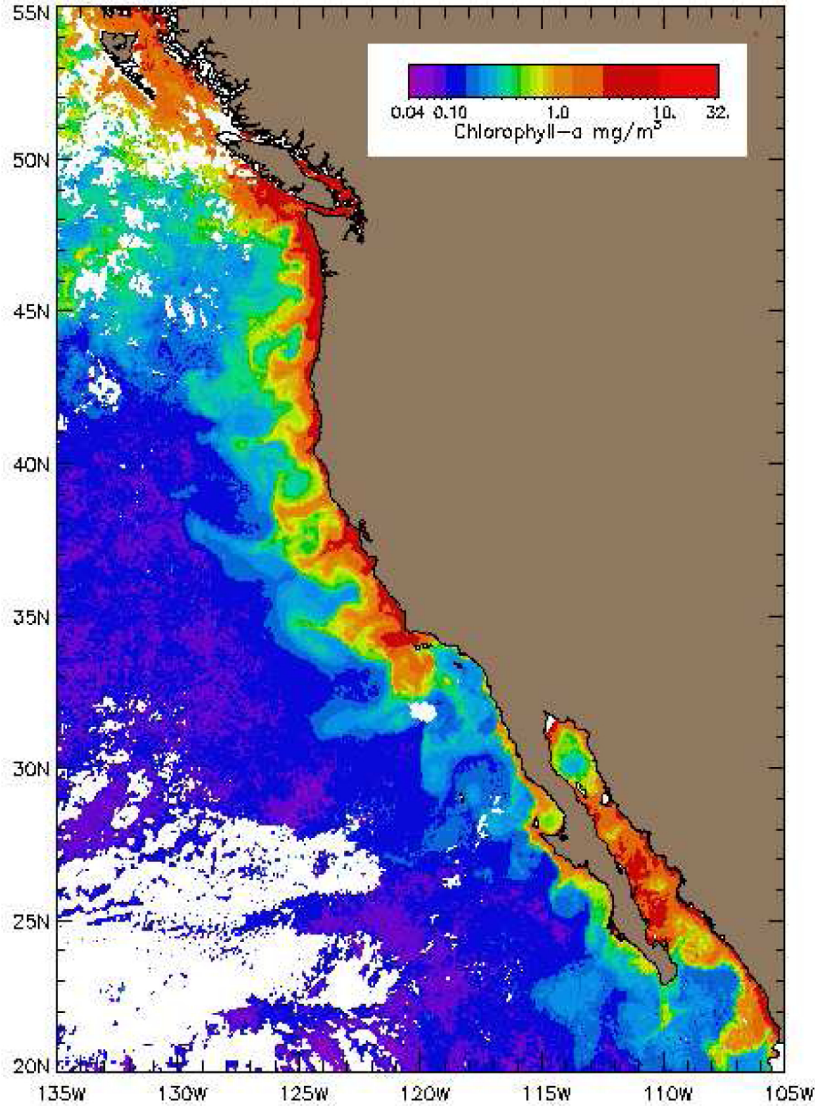


FIGURE 2. “SeaWiFS satellite image of the North American Pacific coast showing the occurrence of coastal upwelling from Baja California (Mexico) to Vancouver Island (Canada). Colors indicate the amount of chlorophyll concentration in the water, with high values (red and orange colors) in regions of high biological activity and low values (blue and purple colors) in biologically inactive waters. Note how instabilities greatly distort the upwelling front (transition from yellow to light blue color). (Compositeimage provided courtesy of Dr. Andrew Thomas, School of Marine Sciences, University of Maine, USA.)” [CRB10]

equations (1) - (3) describe upwelling and downwelling.

$$(1) \quad \frac{\partial v}{\partial t} + \frac{\partial \psi}{\partial z} \frac{\partial v}{\partial x} - \frac{\partial \psi}{\partial x} \frac{\partial v}{\partial z} + \frac{\partial \psi}{\partial z} = \pm 1$$

$$(2) \quad \frac{\partial \rho}{\partial t} + \frac{\partial \rho}{\partial x} \frac{\partial \psi}{\partial z} - \frac{\partial \psi}{\partial x} \frac{\partial \rho}{\partial z} = 0$$

$$(3) \quad \left(1 + \frac{\partial v}{\partial x}\right) \frac{\partial^2 \psi}{\partial t^2} + 2 \frac{\partial \rho}{\partial x} \frac{\partial^2 \psi}{\partial x \partial z} - \frac{\partial \rho}{\partial z} \frac{\partial^2 \psi}{\partial x^2} = 0$$

where v is alongshore velocity, ρ is the density anomaly, ψ is the stream function, x is the cross-slope coordinate, and z the vertical coordinate. In equation (1), +1 models upwelling, while the -1 models downwelling. The equations represent the conservation of momentum (1) and density (2) following the cross-shore flow in the deep frictionless interior below the surface Ekman layer. For California, cross-shore refers to the east-west dimension and alongshore is defined as the north-south dimension. The Ekman layer is the turbulent water due to wind stress on the ocean's surface, as seen in Figure 1. [Gil82]

This is a two dimensional model. When we consider a specific case of upwelling or downwelling, it is for a vertical cross-section of coastline. It is as if the coast of California is a loaf of bread. We look at individual slices to study the phenomena's behaviors. Each slice is the xz -plane.

Flow from the surface layer into or out of the deep interior is modelled by a point source or sink at the origin, meaning that fluid is being injected or removed. To illustrate the downwelling case, imagine we connect a hose to the origin a turn it on full blast so that well-mixed water is forced into our model. Equation (3) is the requirement on the stream function to ensure thermal wind balance holds. [Ped78]

III. THERMAL WIND

Thermal wind balance accounts for geostrophic and hydrostatic balance. A system is in hydrostatic balance when the pressure on a fluid parcel is equal to the weight of the fluid above it. This can be displayed by the equation

$$(4) \quad \frac{\partial p}{\partial z} = -\rho g,$$

where p is pressure, z is the depth, ρ is density and g is acceleration due to gravity. Perhaps a more familiar form of the equation is when we integrate with respect to z , yielding

$$(5) \quad -g \int \rho dz = p.$$

Equation (4) holds when the fluid is static or in a system slowly approaching equilibrium. See Figure 3. It is a good approximation for slow moving fluid and works for physical processes in most oceanic models.

Because the Earth is a non-inertial reference frame, we must insert an extra term onto Newton's laws to describe fluid motion. This term accounts for the Coriolis force. The Coriolis force is dependent on velocity of the fluid parcel. It acts perpendicularly to the velocity vector. A particle in the Northern Hemisphere is turned to its right by the Coriolis force. It is turned to its left in the Southern Hemisphere. It is important in situations where a particle is moving very quickly or it is moving over a long period of time, allowing the

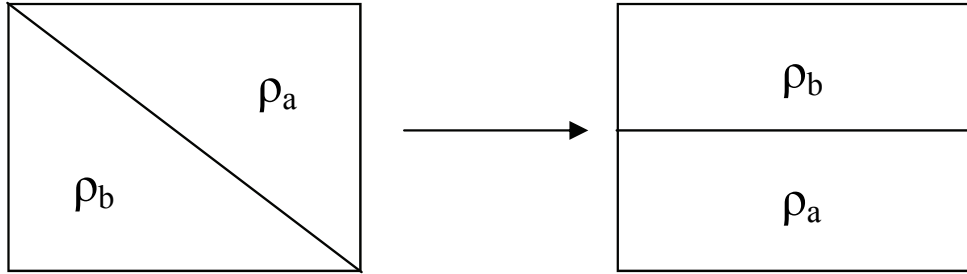


FIGURE 3. Hydrostatic balance is illustrated. Imagine we have a large container with two regions of fluid with different densities. Suppose $\rho_a > \rho_b$. The container on the left is out of equilibrium. The fluids will orient themselves so that the denser fluid is on the bottom of the container.

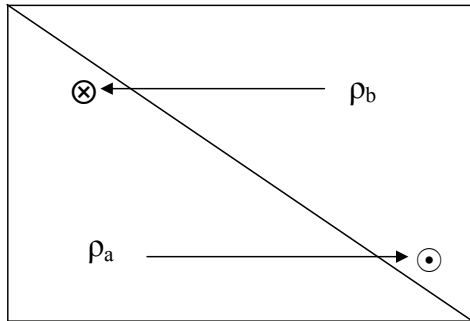


FIGURE 4. Geostrophic balance and thermal wind are illustrated. Imagine we have a large container with two regions of fluid with different densities, similar to Figure 3, but incorporating Coriolis effects. Suppose $\rho_a > \rho_b$. As the system approaches equilibrium, a fluid parcel in region A with a velocity to the right will experience a Coriolis force that turns it to its right, into the page. Similarly, a fluid parcel from region B with velocity to the left will experience a force to its right, out of the page.

Coriolis force to have a significant effect. [Ped78] To see how combination of geostrophic and hydrostatic balance work together, see Figure 4.

Geostrophic balance is equilibrium between the Coriolis force and the pressure gradient. For example, fluid tends to rush into a low pressure center, but in doing so, experiences an acceleration due to the Coriolis force pushing it to its right. Thus, the fluid is pushed around the low pressure center in a circular motion. A hurricane is an example of this behavior. This concept is illustrated in Figure 5.

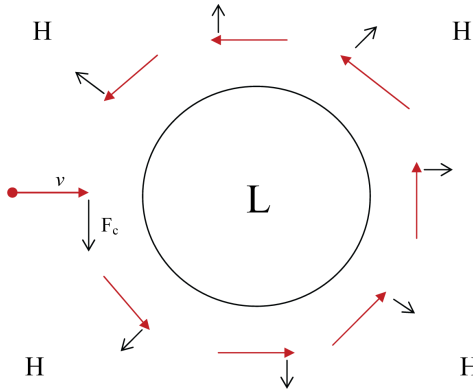


FIGURE 5. Illustration of the Coriolis force. The fluid parcel approaching on the left is drawn from a high pressure region into the low pressure center, as indicated by the red arrows. Since it undergoes an acceleration during this process, the Coriolis force arises, shown in this figure with black arrows. The fluid parcel is pushed to its right by the Coriolis force. This process continues, resulting in the parcel being rotated about the low pressure center.

Geostrophic balance is given by equations (6) and (7),

$$(6) \quad fv = \frac{1}{\rho} \frac{\partial p}{\partial x}$$

$$(7) \quad fu = -\frac{1}{\rho} \frac{\partial p}{\partial y}.$$

Here, v is the velocity into the page, and f is a parameter describing the Coriolis force, which is treated as a constant. The variable x represents the cross-shore direction (east-west) and y is alongshore distance (north-south). The ocean may be treated as a large scale system where the fluid tends towards geostrophic balance on time scales longer than a day.

It is appropriate to consider the Rossby number when determining if a system is in geostrophic balance. The Rossby number is given by equation (8),

$$(8) \quad R_0 = \frac{U}{fL}.$$

Here, U is the velocity of a fluid parcel, f is the Coriolis parameter, and L is a length scale. If the Rossby number is small, we can neglect acceleration terms in the equations of motions before any modeling assumptions are made. Then the system is considered to be in geostrophic balance. [Ped78] The Rossby number is commonly used by physical oceanographers and has to do with the nondimensionalization of the equations.

The model we worked with is unique in that it is only geostrophic in one direction because of the differing velocities and length scales. We assumed that our alongshore length was infinite and the alongshore velocity

was very high. Cross-shore velocity is much smaller, and the cross-shore length scale is finite, therefore much shorter than the alongshore direction. We take the Rossby number to be equal to one in the cross shore direction and small in the alongshore direction. [CSA05]

To get thermal wind balance, we differentiate p with respect to x in (4) and with respect to z in (6). Since the model is nondimensional, f and g and scaled to 1. Equating mixed partials, we arrive at the thermal wind relation,

$$(9) \quad \frac{\partial v}{\partial z} = -\frac{\partial \rho}{\partial x}.$$

The important thing to take away from this discussion is that thermal wind is not a literal breeze. It is a mathematical relationship between density and velocity that accounts for modeling assumptions of geostrophic and hydrostatic balance.

IV. SOLUTIONS

Solutions were originally discovered for upwelling over an idealized flat bottom bathymetry and vertical coastal wall, [CSA05]

$$\begin{aligned} \psi(x, z) &= \frac{2}{\pi} \tan^{-1} \left(\tanh \frac{\pi x}{2} \cot \frac{\pi z}{2} \right) \\ \rho(x, z, t) &= \frac{1}{\pi} \cos^{-1} \left(\cos \pi z - \frac{\sin^2 \pi z [1 - \exp(-\pi t)]}{\cosh \pi x - \cos \pi z} \right) \\ v(x, z, t) &= t - x - \frac{1}{\pi} \cosh^{-1} \left(\cosh \pi x + \frac{\sinh^2 \pi x [\exp(\pi t) - 1]}{\cosh \pi x - \cos \pi z} \right). \end{aligned}$$

Notice that the stream function, ψ , is constant in time. This allows us to treat any streamline as the bottom bathymetry. Using this fact, the solutions may be generalized to account for a family of bottom bathymetries, z_B , where each bathymetry is actually a contour of the stream function. This results in the following solutions for upwelling:

$$\begin{aligned}\psi(x, z) &= \frac{1}{\mu} \tan^{-1} (\tanh \mu x \cot \mu z) + 1 - \frac{\pi}{2\mu} \\ \rho(x, z, t) &= \frac{1}{2\mu} \cos^{-1} \left(\cos 2\mu z - \frac{\sin^2 2\mu z [1 - \exp(-2\mu t)]}{\cosh 2\mu x - \cos 2\mu z} \right) \\ v(x, z, t) &= t - x - \frac{1}{2\mu} \cosh^{-1} \left(\cosh 2\mu x + \frac{\sinh^2 2\mu x [\exp(-2\mu t) - 1]}{\cosh 2\mu x - \cos 2\mu z} \right) \\ z_B(x) &= \frac{1}{\mu} \tan^{-1} (S \tanh \mu x), \quad \mu = \tan^{-1} S\end{aligned}$$

The corresponding downwelling solutions are discovered by the transformations $t \rightarrow -t$ and $\psi \rightarrow -\psi$, effectively reversing time and direction of flow. The solutions for downwelling are written as:

$$(10) \quad \psi(x, z) = -\frac{1}{\mu} \tan^{-1} (\tanh \mu x \cot \mu z) - 1 + \frac{\pi}{2\mu}$$

$$(11) \quad \rho(x, z, t) = \frac{1}{2\mu} \cos^{-1} \left(\cos 2\mu z - \frac{\sin^2 2\mu z [1 - \exp(2\mu t)]}{\cosh 2\mu x - \cos 2\mu z} \right)$$

$$(12) \quad v(x, z, t) = -t - x - \frac{1}{2\mu} \cosh^{-1} \left(\cosh 2\mu x + \frac{\sinh^2 2\mu x [\exp(2\mu t) - 1]}{\cosh 2\mu x - \cos 2\mu z} \right)$$

$$(13) \quad z_B(x) = \frac{1}{\mu} \tan^{-1} (S \tanh \mu x), \quad \mu = \tan^{-1} S$$

Note that the stream function, (10), remains constant in time. In the mixed layers, the arguments of \cos^{-1} in (11) and \cosh^{-1} in (12) are outside of the domain of these inverse functions. In this case, we make the arguments equal to one. This consistency of this condition is demonstrated in Appendix B. In (13), S is a nondimensionalized slope Burger number, giving slope of z_B at the origin. [CSA05] Slope Burger number is a commonly used parameter that relates to nondimensionalization to be discussed later.

The downwelling model contains many rich structures worthy of in-depth investigation. We concentrated much of our efforts on the mixed region. Water of constant density enters the domain through the point source at the origin. This fluid may be considered well-mixed by the turbulence in the surface Ekman layer. Well-mixed means we can consider the fluid to be of constant density and for this case, set $\rho = 0$. In the mixed region, the solutions for ρ and v do not hold, but are replaced by $\rho = 0, v = -t - x$. This is also a result of setting the arguments of (11) and (12) equal to 1. A characteristic plot of downwelling is presented in Fig.6.

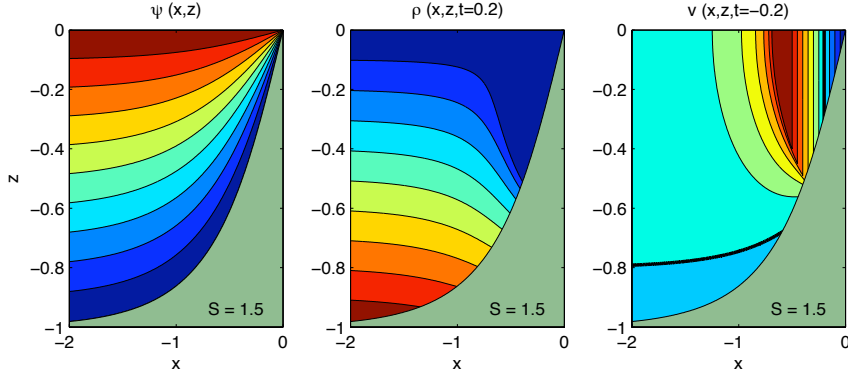


FIGURE 6. A characteristic plot of downwelling, modeled by the analytic function. These plots represent the stream function, density, and velocity, respectively, in nondimensional units. In the velocity plots, the red regions represent northward along slope fluid flow. The mixed region can be clearly seen in the velocity plot. It is the rainbow colored region with vertical contours. The shape of the mixed region can be seen in the density plot, indicating that all water in the mixed region is of uniform density. The bold black line in the velocity plot is the zero contour. Fluid parcels above this line have a net northward alongshore velocity while fluid parcels below the line flow southward.

V. THE STREAM FUNCTION

A stream function represents the flow lines for the fluid parcels. It is defined by equations in (14), which relate the stream function, ψ , to the cross-shore velocity, u , and the vertical velocity, w .

$$(14) \quad u = \frac{\partial \psi}{\partial z}, \quad w = -\frac{\partial \psi}{\partial x}$$

Think of ψ as the path of the fluid. See Figure 7. In general, a stream function describes lines that a particle subject to a vector field follows. For fluid mechanics, velocity vectors are tangent to the flow lines. The units of the stream function are $[\Psi] = \frac{m^2}{s}$. The equation of the stream function (10) satisfies Laplace's equations $\nabla^2 \psi = 0$. This is common for fluid models where fluid is being advected on a large scale without any extraneous point sources or sinks.

By itself, the numerical value of ψ has little significance, but it is illuminating to note that the difference in the stream function represents a volume flux. While volume can change, mass and momentum are conserved. The stream function is analogous to an electric field. It makes more physical sense to talk about the potential difference between points than consider potential at a single point. For downwelling, the stream function indicates net offshore flow. Upwelling is the opposite.

The stream function is the key to the model's dependence on slope. The individual contours of the stream function can be treated as various bathymetries. After a contour is chosen to be used as bathymetry, rest of the stream function is scaled from 0 to -1.

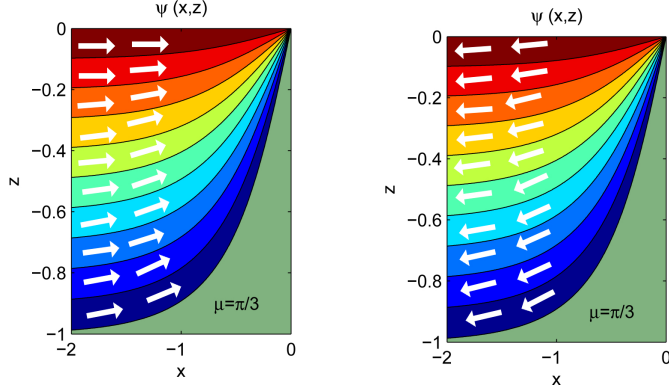


FIGURE 7. The stream functions for upwelling and downwelling compared. Arrows pointing left represent westward flow out to sea for the downwelling case. Upwelling is represented by arrows pointing to the right. The colors represent contours. A particle will stay in the same contour as it is advected out to sea or to the origin. Recall, this is a non-dimensional model so the axis have no units. To get an idea of scale, the z-axis depth is usually on the order of hundreds of meters while the x-axis is on the order of several kilometers.

The slope Burger number is a parameter commonly in physical oceanography by researchers who study coastal phenomena. The Burger number relates the slope of the bathymetry at the coast to the buoyancy frequency. It is given by the equation

$$(15) \quad S = \frac{N\alpha}{f},$$

where N represents buoyancy frequency, α is the slope of the bathymetry at the coast, and f is the Coriolis parameter. [LC04] One aspect of this research was to examine how the rescaling of the stream function affects various features common to downwelling such as the propagation of the mixed region.

VI. SUMMARY OF WORK

We set out to confirm that the upwelling and downwelling solutions (10)-(12) satisfy the partial differential equations (1)-(3) when modified to include bottom bathymetry. Using algebraic techniques and mathematical software, we explored various features of the downwelling model, including the shape and dynamics of the mixed region, how slope affected the development of typical features, and the appearance of a southward undercurrent. Finally, we compared our analytical solutions with the 2-Dimensional Princeton Ocean Model [BM87] to determine how well the model articulated understood features of downwelling.

VII. ALGEBRAIC METHODS

It was verified that the analytical solutions satisfy the differential equations for upwelling and downwelling through direct substitution into (1), (2), and (3). The mathematical software, Maple, was used to aid in

these long calculations, particularly in taking the partial derivatives of the solutions. However, the bulk of the simplifications and algebraic manipulations required were done by hand to ensure accuracy. The procedure was similar for the upwelling and downwelling solutions. In particular, isolating the terms

$$(16) \quad \rho_{arg} = \left(\cos 2\mu z - \frac{\sin^2 2\mu z [1 - \exp(2\mu t)]}{\cosh 2\mu x - \cos 2\mu z} \right)$$

$$(17) \quad \xi_{arg} = \left(\cosh 2\mu x + \frac{\sinh^2 2\mu x [\exp(-2\mu t) - 1]}{\cosh 2\mu x - \cos 2\mu z} \right)$$

and replacing variables of the form $2\mu x$, $2\mu z$, $2\mu t$ with \bar{x} , \bar{z} , and \bar{t} , respectively, helps ease the simplifications and makes the necessary reductions more visible. See Appendix C.

Setting $\rho_{arg} = \xi_{arg} = 1$ gives an equation describing the front of the mixed region for any time. While these equations appear to be very different, after creating a brief Maple animation of the front growing over time, we observed that they were numerically equivalent within the xz -plane; we then verified this fact algebraically. Refer to Appendix B for further information on the algebraic manipulation. Further utilizing Maple's animation capabilities, we compared the region with an ellipse centered at the origin and intersecting the x -axis and z -axis at the appropriate position atop the previously created animation and determined numerically that the region was not a conical ellipse, as the plot is more convex than a normal ellipse.

VIII. NOTABLE FEATURES

We modified the Matlab files from the flat bottom upwelling solution to account for sloping bathymetry. Since the stream function is time independent, we can treat any of its contours as bottom bathymetry and scale the model's features appropriately. See Figure 9. We then adjusted for downwelling by making the transformations $t \rightarrow -t$ and $\psi \rightarrow -\psi$. With the Matlab generated plots, we were able to see how the analytical model would behave given certain slopes and times. A time progression of the model can be seen in Figure 8. Features of interest were then investigated algebraically.

For steep slopes, the mixed region propagates more slowly. Recall the colloquialism, "Still waters run deep." This applies quite literally in explaining the cross-shore velocity of the mixed region. The mass flux from fluid introduced at the point source is constant. For shallow slopes, the same mass of fluid is being forced through a smaller region so it must travel at a higher cross-shore velocity. Four particular slopes are shown in Figure 9.

Most notably, a southward undercurrent oriented out of the page is observed in several plots of downwelling with sloping bottom bathymetry. This undercurrent is not always immediately visible above the bottom

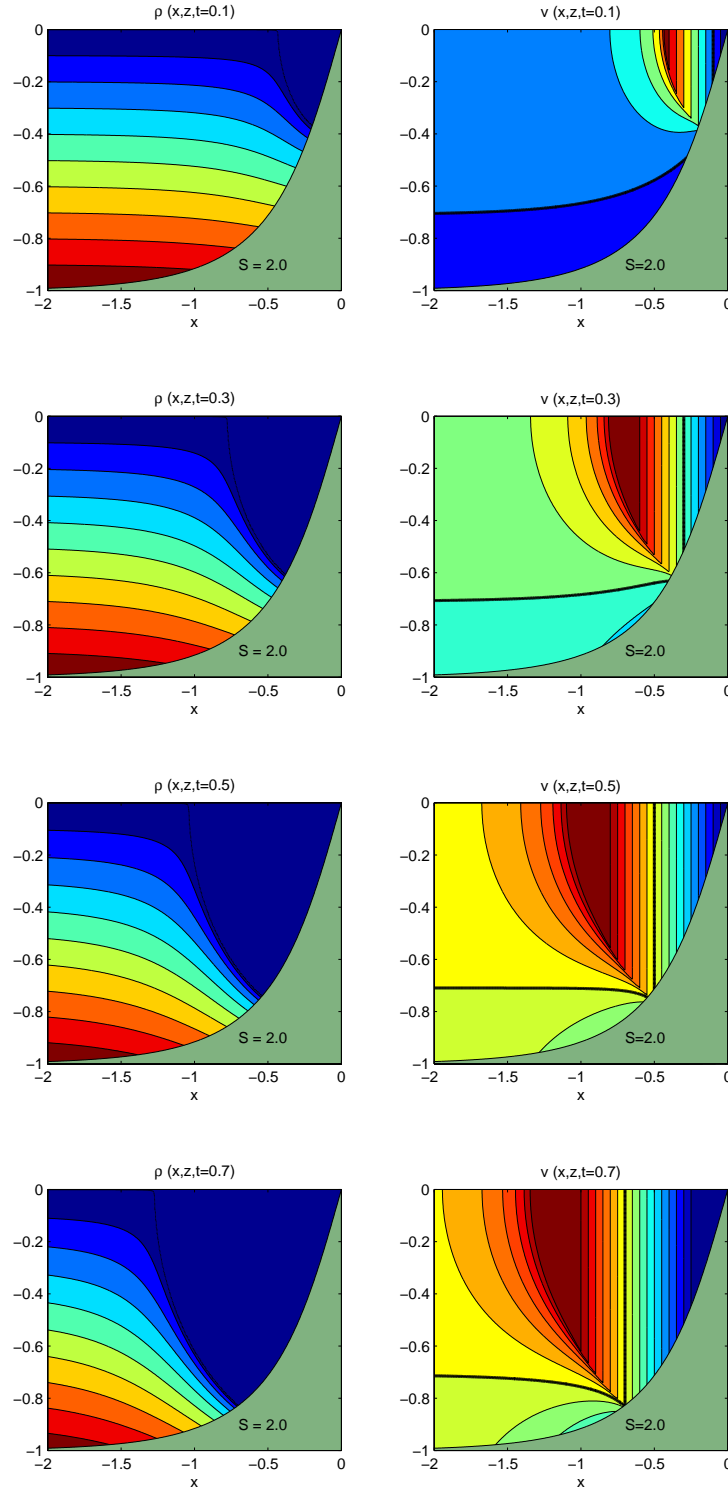


FIGURE 8. The time progression of the bottom bathymetry $S = 2.0$. It illustrates the development of characteristic regions expected for downwelling. In the velocity plot, notice the mixed region, the zero velocity contour, and the southern undercurrent development.

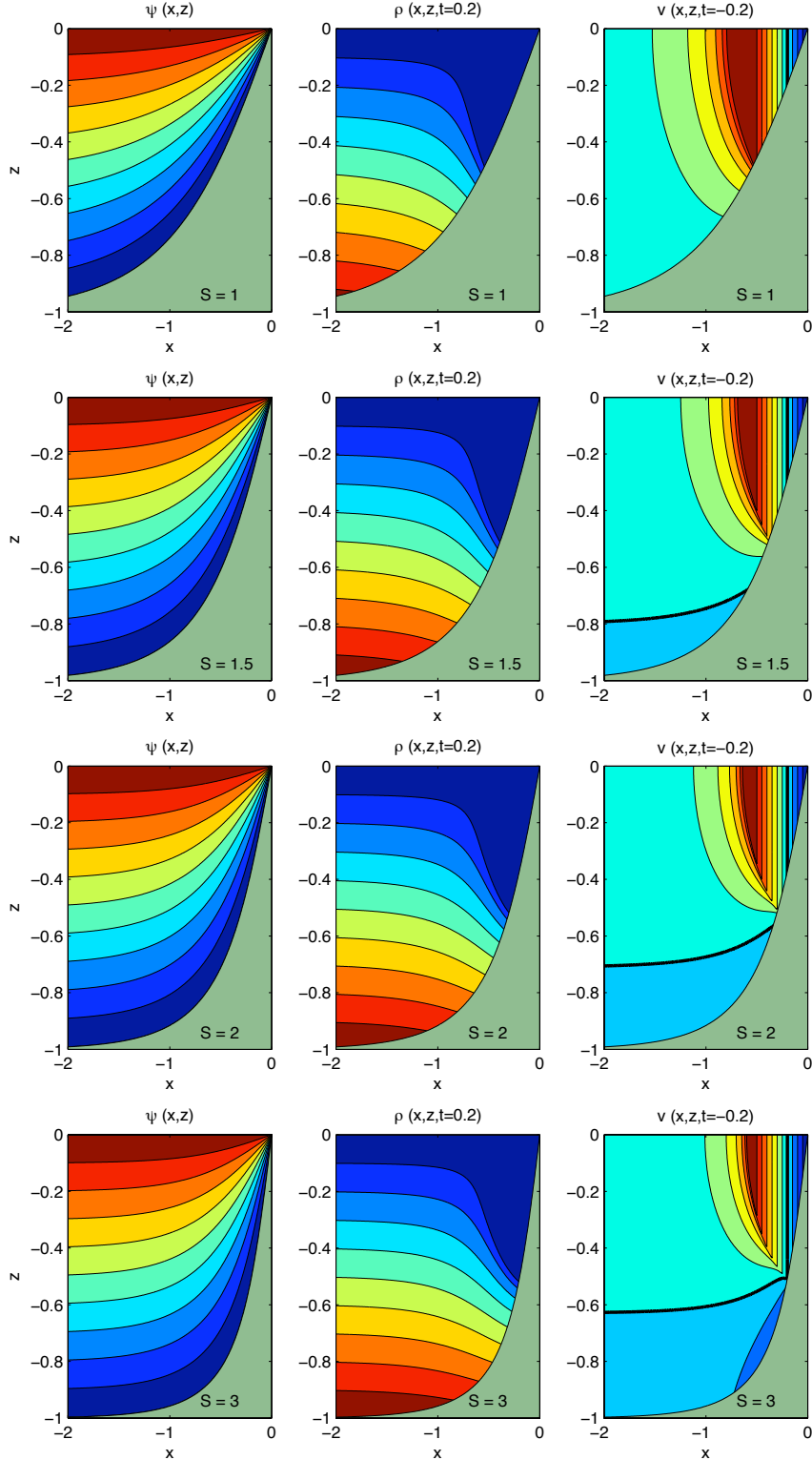


FIGURE 9. Downwelling after approximately six days modeled over bathymetries where $S = 1, 1.5, 2.0, 3.0$. Note that the mixed region has propagated further off shore for the shallower slopes. The southern undercurrent has not yet formed for any case other than $S = 3.0$. These plots also display the stretching of the stream function and its use as generalized bottom bathymetry.

bathymetry and sometimes does not emerge above it at all. For an undercurrent to form and be visible above the bottom bathymetry, the zero contour of the cross-slope velocity must emerge above the bottom bathymetry. Taking the limit as $x \rightarrow -\infty$ of the zero contour of cross-slope velocity ($v(x, z, t) = 0$),

$$(18) \quad 2\mu z = \arccos \left(\frac{-\exp(-2\mu t) \sinh^2(2\mu x) + \cosh(2\mu x) \cosh(2\mu t + 2\mu x)}{\cosh(2\mu t + 2\mu x) - \cosh(2\mu x)} \right),$$

gives $z = \frac{-\pi}{4\mu}$. Thus, whenever the slope, μ , makes this $z > z_B$, some portion of the undercurrent will eventually become visible above the bottom bathymetry. This shows that the undercurrent will be more apparent for larger values of μ , giving smaller values of z . This assertion is rigorously proved in Appendix A.

The southern undercurrent forms because of the assumption of a southern pressure gradient. We imposed this pressure gradient as -1 in equation (1). For shallow slopes, that is $\mu < \frac{\pi}{4}$, there is a strong cross-shore velocity, u , so the Coriolis force dominates and generate a net northward flow in v . For steep slopes, there is a smaller cross-shore velocity so the pressure gradient is the dominant term. Thus, the alongshore velocity v is negative which corresponds to a southward oriented flow.

IX. COMPARISON TO A NUMERICAL MODEL

Fortran was used to compile data from the Princeton Ocean Model which we used to compare with our solution in Matlab. The Princeton Ocean Model was modified to run in two dimensions (POM2D), cross-shore and depth, and simulations of downwelling were run to compare with the analytic solutions. See Figure 10 for an example of a typical POM2D plot. Simulations were run without bottom friction, but retained the surface Ekman layer. POM2D includes dynamics such as a free surface and advection of cross-shore momentum not included in the Pedlosky model. The advection of fluid also differs in POM2D because it circulates the fluid from the Ekman layer. As mentioned previously, the flow from the surface Ekman layer is modeled by a point source or sink in the analytical model. For the downwelling case, it is a point source. This is significantly different from POM2D and accounts for some of the differences that arise in the comparison. POM2D exhibits a continuously growing mixed layer at the surface, while the analytical solutions, by using a point source, do not include this growing layer. Thus, as time increases, plots from the numerical model deviate from picture given by the analytical model.

Three main regions of interest in our downwelling model are the mixed region, the zero contour, and the southward undercurrent. We observed that the shape of the mixed region appeared elliptical, but discovered a solution that showed it was not the case. The mixed region is modeled by $\rho_{arg} = \xi_{arg} = 1$ analytically, but this is not a good fit for the numerical simulation. In POM2D, we found that the shape of the mixed region differs and propagates at a slower rate. The differences are exhibited in Figure 11.

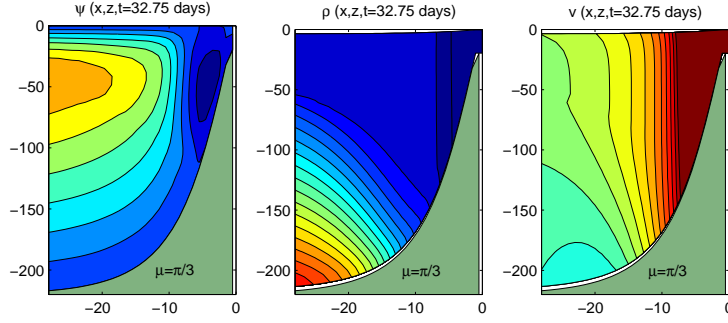


FIGURE 10. A characteristic plot of downwelling for POM2D. Note that ψ , the stream function, includes a circulating Ekman layer, accounting for the difference with the numerical model. Time is set for 32.75 days, which is uncommonly long for a real downwelling event. The units on the vertical are meters and the horizontal is in kilometers. Also note the development of a southern undercurrent in the velocity plot.

While the details of the mixed region in downwelling are not captured well by the POM2D solutions, the deep undercurrent is generated for steep slopes in both the analytical model and numerical solutions. The feature is apparent in Figure 11. We made the same modeling assumptions in both cases, so this reinforces the conclusion that the current's formation is due to thermal wind balance, the southward pressure gradient, and alongshore uniformity.

X. CONCLUDING REMARKS

This project deals with the exploration of new solutions to a system of nonlinear, coupled partial differential equations that describe the advection of fluid parcels. Unlike the previously published solution [CSA05], this model works for a wide range of bottom slopes. The model predicts how a sloped bottom bathymetry can affect the phenomena of upwelling and downwelling. The dynamic consequences of our assumptions, thermal wind balance and alongshore uniformity, pinpoint causes for some observed phenomena. This solution has untapped potential for further exploration in the field of physical oceanography within the context of instability development.

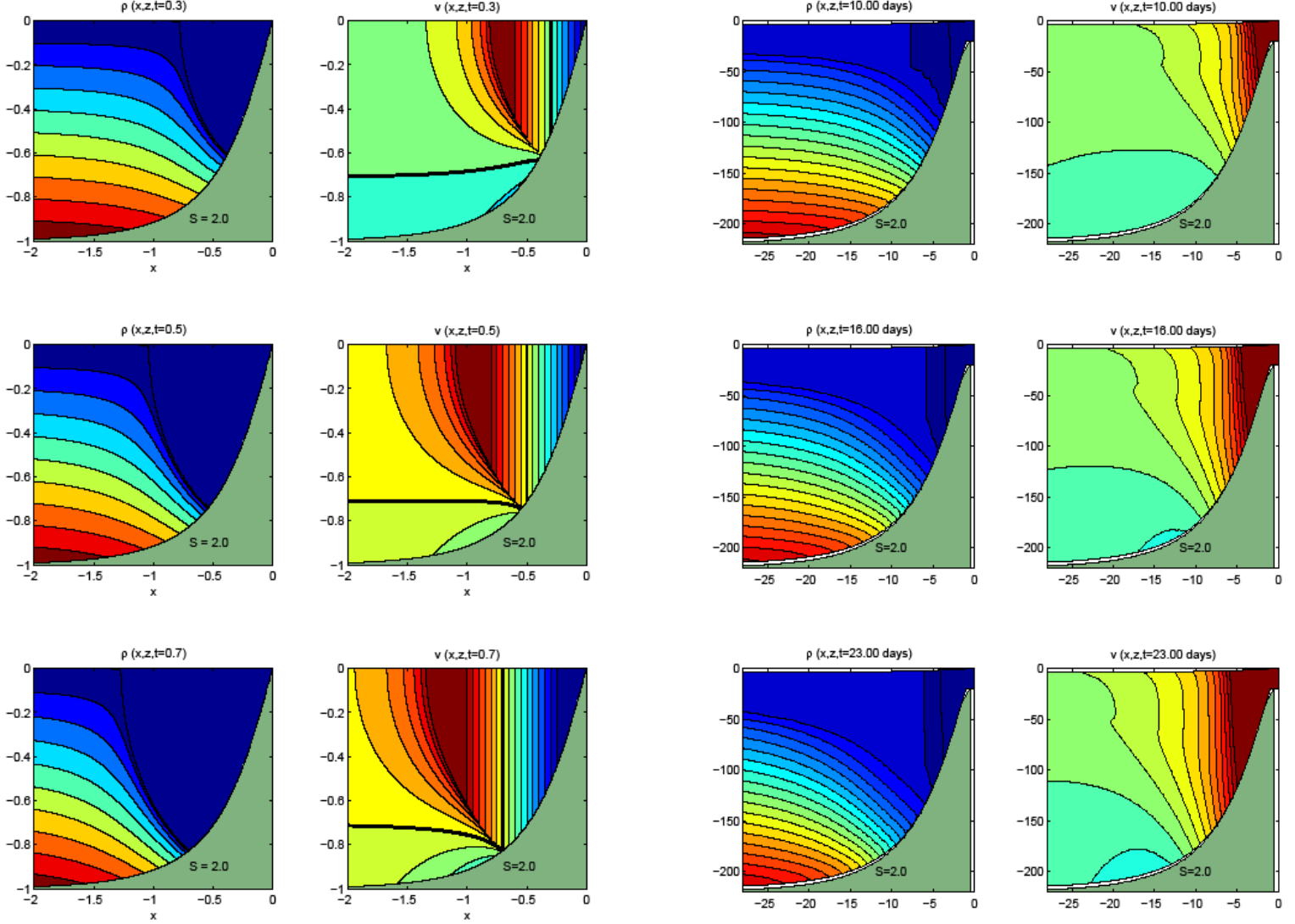


FIGURE 11. Time progressions (10 days, 16 days, and 23 days) are shown here comparing density and along slope velocity between the analytical (left) and numerical models (right). Significant differences can be seen in the progression of the mixed region on the density plots. Notice the southward undercurrent at the bottom of the velocity plots forms in a similar manner in both models.

APPENDIX A. THE ZERO-CONTOUR OF $v(x, z, t)$

Here we investigate the zero-contour of $v(t, x, z)$ for downwelling. This is of interest because we wish to determine which slopes for which the southward undercurrent will eventually form. We will find an equation, solving for \bar{z} , then take a limit to see how the contour changes then compare to $z_B(x)$ in order to see for which slopes the undercurrent eventually appears. Note that we have used $\bar{x}, \bar{t}, \bar{z}$ to represent $2\pi x, 2\pi t,$

and $2\pi z$, respectively.

$$(19) \quad 0 = -t - x - \frac{1}{2\mu} \cosh^{-1} \left(\cosh(\bar{x}) + \frac{\sinh(\bar{x})(e^{-\bar{t}} - 1)}{\cosh(\bar{x} - \cos(\bar{z}))} \right)$$

$$(20) \quad \cosh(\bar{t} + \bar{x}) - \cosh(\bar{x}) = \frac{\sinh^2(\bar{x})(e^{-\bar{t}} - 1)}{\cosh(\bar{x}) - \cos(\bar{z})}$$

$$(21) \quad \cosh(\bar{x})(\cosh(\bar{t} + \bar{x}) - \cosh(\bar{x})) - \cos(\bar{z})(\cosh(\bar{t} + \bar{x}) - \cosh(\bar{x})) = \sinh^2(\bar{x})(e^{-\bar{t}} - 1)$$

$$(22) \quad -\cos(\bar{z})(\cosh(\bar{t} + \bar{x}) - \cosh(\bar{x})) = \sinh^2(\bar{x})(e^{-\bar{t}} - 1) - \cosh(\bar{x})(\cosh(\bar{t} + \bar{x}) - \cosh(\bar{x}))$$

Note that $-\sinh^2(\bar{x}) + \cosh^2(\bar{x}) = 1$ after distributing.

$$(23) \quad \cos(\bar{z}) = \frac{-e^{-\bar{t}} \sinh^2(\bar{x}) + \cosh(\bar{x}) \cosh(\bar{t} + \bar{x})}{\cosh(\bar{t} + \bar{x}) - \cosh(\bar{x})}$$

$$(24) \quad \bar{z} = \cos^{-1} \left(\frac{-e^{-\bar{t}} \sinh^2(\bar{x}) + \cosh(\bar{x}) \cosh(\bar{t} + \bar{x})}{\cosh(\bar{t} + \bar{x}) - \cosh(\bar{x})} \right)$$

Now let's take the limit as $x \rightarrow -\infty$ to see what the zero-contour approaches.

$$(25) \quad \lim_{x \rightarrow -\infty} \cos^{-1} \left(\frac{-e^{-\bar{t}} \sinh^2(\bar{x}) + \cosh(\bar{x}) \cosh(\bar{t} + \bar{x})}{\cosh(\bar{t} + \bar{x}) - \cosh(\bar{x})} \right)$$

Converting the hyperbolic function to exponentials we have,

$$(26) \quad = \lim_{x \rightarrow -\infty} \cos^{-1} \left(\frac{-e^{-\bar{t}} \frac{1}{4}(e^{\bar{x}} - e^{-\bar{x}})^2 + \frac{1}{2}(e^{\bar{x}} + e^{-\bar{x}}) \frac{1}{2}(e^{\bar{t}+\bar{x}} + e^{-\bar{t}-\bar{x}})}{\frac{1}{2}(e^{\bar{t}+\bar{x}} + e^{-\bar{t}-\bar{x}}) - \frac{1}{2}(e^{\bar{x}} + e^{-\bar{x}})} \right)$$

Since \cos^{-1} is continuous we may move the limit inside its argument

$$(27) \quad = \cos^{-1} \left(\lim_{x \rightarrow -\infty} \frac{-e^{-\bar{t}} \frac{1}{2}(e^{2\bar{x}} + e^{-2\bar{x}} - 2) + \frac{1}{2}(e^{\bar{t}} e^{2\bar{x}} + e^{-\bar{t}} + e^{\bar{t}} + e^{-\bar{t}} e^{-2\bar{x}})}{e^{\bar{t}} e^{\bar{x}} + e^{-\bar{t}} e^{-\bar{x}} - e^{\bar{x}} - e^{-\bar{x}}} \right)$$

$$(28) \quad = \cos^{-1} \left(\lim_{x \rightarrow -\infty} \frac{-\frac{1}{2}e^{-\bar{t}}e^{2\bar{x}} - \frac{1}{2}e^{-\bar{t}}e^{-2\bar{x}} + e^{-\bar{t}} + \frac{1}{2}e^{\bar{t}}e^{2\bar{x}} + \frac{1}{2}e^{-\bar{t}} + \frac{1}{2}e^{\bar{t}} + \frac{1}{2}e^{-\bar{t}}e^{-2\bar{x}}}{e^{\bar{x}}(e^{\bar{t}} - 1) + e^{-\bar{x}}(e^{-\bar{t}} - 1)} \right)$$

$$(29) \quad = \cos^{-1} \left(\lim_{x \rightarrow -\infty} \frac{e^{2\bar{x}}(-\frac{1}{2}e^{-\bar{t}} + \frac{1}{2}e^{\bar{t}}) + e^{-\bar{t}} + \frac{1}{2}e^{-\bar{t}} + \frac{1}{2}e^{\bar{t}}}{e^{\bar{x}}(e^{\bar{t}} - 1) + e^{-\bar{x}}(e^{-\bar{t}} - 1)} \right)$$

Holding all terms without an x to be constant, we may rewrite this as

$$(30) \quad = \cos^{-1} \left(\lim_{x \rightarrow -\infty} \frac{e^{2\bar{x}}c_1 + c_2}{e^{\bar{x}}c_3 + e^{-\bar{x}}c_4} \right)$$

Where each c_i is a constant. Now taking the limit we see that the numerator goes to a constant and the denominator goes to infinity, giving us

$$(31) \quad \lim_{x \rightarrow -\infty} \bar{z} = \cos^{-1}(0) = \pm \frac{\pi}{2}$$

Substituting $\bar{z} = 2\mu z = -\frac{\pi}{2}$,

$$(32) \quad z = -\frac{\pi}{4\mu}$$

As a sanity check, substituting $\mu = \frac{\pi}{2}$ for the flat bottom case we have $z = -\frac{1}{2}$, which is of course the expected value for the zero-contour as $x \rightarrow -\infty$. Now notice that

$$(33) \quad \lim_{x \rightarrow -\infty} z_B = \lim_{x \rightarrow -\infty} \frac{1}{\mu} \tan^{-1}(S \tanh(\mu x))$$

$$(34) \quad = \frac{1}{\mu} \tan^{-1} \left(\lim_{x \rightarrow -\infty} S \frac{e^x - e^{-x}}{e^x + e^{-x}} \right)$$

$$(35) \quad = \frac{1}{\mu} \tan^{-1}(-S)$$

Now substituting $S = \tan(\mu)$

$$(36) \quad = \frac{1}{\mu} \tan^{-1}(-\tan(\mu))$$

Which gives us

$$(37) \quad \lim_{x \rightarrow -\infty} z_B = -1$$

So we see that at $\mu = \frac{\pi}{4}$, $z = -1$ for z_B as well as in the limit of the zero-contour, making this slope the boundary case for when the undercurrent eventually appears.

APPENDIX B. THE FRONT OF THE MIXED REGION

We now confirm that $\rho_{arg} = \xi_{arg}$ at the front of the mixed region. Recall that,

$$(38) \quad \rho_{arg} = \cos(\bar{z}) - \frac{\sin^2(\bar{z})(1 - e^{\bar{t}})}{\cosh(\bar{x}) - \cos(\bar{z})}$$

$$(39) \quad \xi_{arg} = \cosh(\bar{x}) + \frac{\sinh^2(\bar{x})(e^{-\bar{t}} - 1)}{\cosh(\bar{x}) - \cos(\bar{z})}$$

Now setting these equations equal to 1 defines the front of the mixed region. We now attempt to show these are equal. We begin with ρ_{arg} .

$$(40) \quad 1 = \cos(\bar{z}) - \frac{\sin^2(\bar{z})(1 - e^{\bar{t}})}{\cosh(\bar{x}) - \cos(\bar{z})}$$

$$(41) \quad \cosh(\bar{x}) - \cos(\bar{z}) = \cos(\bar{z}) \cosh(\bar{x}) - \cos^2(\bar{z}) - \sin^2(\bar{z})(1 - e^{\bar{t}})$$

Distributing the $\sin^2(\bar{z})$ phrase and substituting $-1 = -\cos^2(\bar{z}) - \sin^2(\bar{z})$,

$$(42) \quad \cosh(\bar{x}) - \cos(\bar{z}) = \cos(\bar{z}) \cosh(\bar{x}) - 1 + \sin^2(\bar{z})e^{\bar{t}}$$

Substituting $1 - \cos^2(\bar{z}) = \sin^2(\bar{z})$ gives

$$(43) \quad \cosh(\bar{x}) - \cos(\bar{z}) = \cos(\bar{z}) \cosh(\bar{x}) - 1 + e^{-\bar{t}} - \cos^2(\bar{z})e^{\bar{t}}$$

Multiplying through by $e^{-\bar{t}}$

$$(44) \quad \cosh(\bar{x})e^{-\bar{t}} - \cos(\bar{z})e^{-\bar{t}} = \cos(\bar{z}) \cosh(\bar{x})e^{-\bar{t}} - e^{-\bar{t}} + 1 - \cos^2(\bar{z})e^{-\bar{t}}$$

Adding $\cos(\bar{z})e^{-\bar{t}}$ and $e^{-\bar{t}}$ to both sides and factoring we have

$$(45) \quad (\cosh(\bar{x}) + 1)e^{-\bar{t}} = \cos(\bar{z})e^{-\bar{t}}(1 + \cosh(\bar{x})) + (1 - \cos^2(\bar{z}))e^{-\bar{t}}$$

Shifting the $\cos(\bar{z})e^{-\bar{t}}(1 + \cosh(\bar{x}))$ term to the left side and factoring

$$(46) \quad (1 + \cosh(\bar{x}))e^{-\bar{t}}(1 - \cos(\bar{z})) = (1 + \cos(\bar{z}))(1 - \cos(\bar{z}))$$

Cancelling the common terms and solving for $\cos(\bar{z})$ we have

$$(47) \quad \boxed{\cos(\bar{z}) = (1 + \cosh(\bar{x}))e^{-\bar{t}} - 1}$$

Now we set ξ_{arg} to 1 and proceed similarly.

$$(48) \quad 1 = \cosh(\bar{x}) + \frac{\sinh^2(\bar{x})(e^{-\bar{t}} - 1)}{\cosh(\bar{x}) - \cos(\bar{x})}$$

$$(49) \quad \cosh(\bar{x}) - \cos(\bar{z}) = (\cosh(\bar{x}) - \cos(\bar{z})) \cosh(\bar{x}) + \sinh^2(\bar{x})(e^{-\bar{t}} - 1)$$

$$(50) \quad \cosh(\bar{x}) - \cos(\bar{z}) = \cosh^2(\bar{x}) - \cos(\bar{z}) \cosh(\bar{x}) - \sinh^2(\bar{x}) + \sinh^2(\bar{x})e^{-\bar{t}}$$

Using the identity $\cosh^2(\bar{x}) - \sinh^2(\bar{x}) = 1$,

$$(51) \quad \cosh(\bar{x}) - \cos(\bar{z}) = 1 - \cos(\bar{z}) \cosh(\bar{x}) + \sinh^2(\bar{x})e^{-\bar{t}}$$

$$(52) \quad \cos(\bar{z}) \cosh(\bar{x}) - \cos(\bar{z}) = 1 - \cosh(\bar{x}) + \sinh^2(\bar{x})e^{-\bar{t}}$$

$$(53) \quad \cos(\bar{z})(\cosh(\bar{x}) - 1) = 1 - \cosh(\bar{x}) + \sinh^2(\bar{x})e^{-\bar{t}}$$

$$(54) \quad \cos(\bar{z}) = \frac{\sinh^2(\bar{x})e^{-\bar{t}}}{\cosh(\bar{x}) - 1} - 1$$

Now substituting in $\sinh^2(\bar{x}) = \cosh^2(\bar{x}) - 1 = (\cosh(\bar{x}) - 1)(\cosh(\bar{x}) + 1)$ we have

$$(55) \quad \cos(\bar{z}) = \frac{(\cosh(\bar{x}) - 1)(\cosh(\bar{x}) + 1)e^{-\bar{t}}}{\cosh(\bar{x}) - 1} - 1$$

Cancelling we have the desired result,

$$(56) \quad \boxed{\cos(\bar{z}) = (1 + \cosh(\bar{x}))e^{-\bar{t}} - 1}$$

APPENDIX C. SUBSTITUTING THE SOLUTIONS INTO THE TRANSFORMED DIFFERENTIAL EQUATIONS

In this section we show that the analytical solutions for upwelling over sloping bathymetry satisfy the first two of the following set of differential equations using transformed variables, as seen in [CSA05],

$$(57) \quad \frac{\partial \xi}{\partial t} + \frac{\partial \xi}{\partial x} \frac{\partial \psi}{\partial z} - \frac{\partial \psi}{\partial x} \frac{\partial \xi}{\partial z} = 0$$

$$(58) \quad \frac{\partial \rho}{\partial t} + \frac{\partial \rho}{\partial x} \frac{\partial \psi}{\partial z} - \frac{\partial \psi}{\partial x} \frac{\partial \rho}{\partial z} = 0$$

$$(59) \quad \xi_x \psi_{zz} + 2\rho_x \psi_{xz} - \rho_z \psi_{xx} = 0.$$

The transformed analytical solutions in transformed variables are given by

$$(60) \quad \psi(x, z) = \frac{1}{\mu} \tan^{-1}(\tanh(\mu x) \cot(\mu z)) + 1 - \frac{\pi}{2\mu}$$

$$(61) \quad \rho(x, z, t) = \frac{1}{2\mu} \cos^{-1} \left(\cos(2\mu z) - \frac{\sin^2(2\mu z)(1 - e^{-2\mu t})}{\cosh(2\mu x) - \cos(2\mu z)} \right)$$

$$(62) \quad \xi(x, z, t) = -\frac{1}{2\mu} \cosh^{-1} \left(\cosh(2\mu x) + \frac{\sinh^2(2\mu x)(e^{2\mu t} - 1)}{\cosh(2\mu x) - \cos(2\mu z)} \right).$$

To ease the process we used the mathematical software, Maple, to determine the partial derivatives and simplify the equations as much as possible. We begin with equation (57), starting with the output from Maple,

$$(63) \quad -\frac{2 \sin^2(2\mu z)\mu e^{-2\mu t}}{\cosh(2\mu x) - \cos(2\mu z)} - \frac{2 \sin^2(2\mu z)(1 - e^{-2\mu t}) \sinh(2\mu x)\mu \sinh(2\mu x)}{(\cosh(2\mu x) - \cos(2\mu z))^3} \\ - \frac{1}{\cosh(2\mu x) - \cos(2\mu z)} \left(\sin(2\mu z) \left(-2 \sin(2\mu z)\mu - \frac{4 \sin(2\mu z)(1 - e^{-2\mu t}) \cos(2\mu z)\mu}{\cosh(2\mu x) - \cos(2\mu z)} \right. \right. \\ \left. \left. + \frac{2 \sin^3(2\mu z)(1 - e^{-2\mu t})\mu}{(\cosh(2\mu x) - \cos(2\mu z))^2} \right) \right).$$

To show that (57) is satisfied, we need to show that this expression is identically 0. This looks daunting, however, substituting in $q = \cosh(\bar{x}) - \cos(\bar{z})$ will make this somewhat more manageable. Note that we return to the $\bar{x}, \bar{z}, \bar{t}$ notation. We also factor out $A = -2\mu \sin^2(\bar{z})/q$ from every term. We list the terms in the same order that they appear above, note also that before factoring terms were distributed completely.

$$(64) \quad = -\frac{2\mu \sin^2(\bar{z})}{q} \left(e^{-\bar{t}} + \frac{(1 - e^{-\bar{t}}) \sinh^2(\bar{x})}{q^2} - 1 - \frac{2(1 - e^{-\bar{t}}) \cos(\bar{z})}{q} + \frac{\sin^2(\bar{z})(1 - e^{-\bar{t}})}{q^2} \right)$$

Notice now that after pairing the free $e^{-\bar{t}}$ and -1 , we may factor out $\frac{(1 - e^{-\bar{t}})}{q^2}$ from each phrase. We include this in A , denoted A'

$$(65) \quad = A' \frac{1 - e^{-\bar{t}}}{q^2} (-q^2 + \sinh^2(\bar{x}) - 2 \cos(\bar{z})q + \sin^2(\bar{z}))$$

Now, after expanding out the q 's inside the parentheses we have

$$(66) \quad = A' (-\cosh^2(\bar{x}) + 2 \cosh(\bar{x}) \cos(\bar{z}) - \cos^2(\bar{z}) + \cosh^2(\bar{x}) - 1 - 2 \cosh(\bar{x}) \cos(\bar{z}) + 2 \cos^2(\bar{z}) + 1 - \cos^2(\bar{z}))$$

Notice that each phrase has an equal and opposite phrase present inside the parentheses, so this simplifies to 0. Thus, the solutions satisfy (57).

We now turn to (58), again starting from the Maple output of plugging in (60)-(62). We start with

$$(67) \quad \frac{2 \sinh^2(2\mu x)\mu e^{2\mu t}}{\cosh(2\mu x) - \cos(2\mu z)} - \frac{1}{\cosh(2\mu x) - \cos(2\mu z)} \left(\left(2 \sinh(2\mu x)\mu \right. \right.$$

$$\left. + \frac{4 \sinh(2\mu x)(e^{2\mu t} - 1) \cosh(2\mu x)\mu}{\cosh(2\mu x) - \cos(2\mu z)} - \frac{2 \sinh^3(2\mu x)(e^{2\mu t} - 1)\mu}{(\cosh(2\mu x) - \cos(2\mu z))^2} \right) \sinh(2\mu x)$$

$$\left. + \frac{2 \sin^2(2\mu z) \sinh^2(2\mu x)(e^{2\mu t} - 1)\mu}{(\cosh(2\mu x) - \cos(2\mu z))^3} \right)$$

Using q again and factoring out $B = 2\mu \sinh^2(\bar{x})/q$ we have

$$(68) \quad = \frac{2\mu \sinh^2(\bar{x})}{q} \left(e^{\bar{t}} - 1 - \frac{2(e^{\bar{t}} - 1) \cosh(\bar{x})}{q} + \frac{\sinh^2(\bar{x})(e^{\bar{t}} - 1)}{q^2} + \frac{\sinh^2(\bar{z})(e^{\bar{t}} - 1)}{q^2} \right)$$

Factoring out $q^2(e^{\bar{t}} - 1)$ and including it in B'

$$(69) \quad = \frac{B(e^{\bar{t}} - 1)}{q^2} (q^2 - 2 \cosh(\bar{x})q + \sinh^2(\bar{x}) + \sin^2(\bar{z}))$$

Expanding out the q 's we have

$$(70) \quad = B' (\cosh^2(\bar{x}) - 2 \cosh(\bar{x}) \cos(\bar{z}) + \cos^2(\bar{z}) - 2 \cosh^2(\bar{x}) + 2 \cosh(\bar{x}) \cos(\bar{z}) + \sinh^2(\bar{x}) + \sin^2(\bar{z}))$$

Cancelling like terms we have

$$(71) \quad = B' (-\cosh^2(\bar{x}) + \sinh^2(\bar{x}) + \cos^2(\bar{z}) + \sin^2(\bar{z}))$$

Using the identities $-\cosh^2(\bar{x}) + \sinh^2(\bar{x}) = -1$ and $\cos^2(\bar{z}) + \sin^2(\bar{z}) = 1$ we see that the argument in the parentheses is 0. Thus, (58) is also satisfied by the solutions. Very similar procedures apply for showing that the solutions also satisfy (59), except that in addition to isolating terms of the form of q , it is also helpful to isolate terms of the form

$$\begin{aligned} \xi_{arg} &= \cosh(\bar{x}) + \frac{\sinh^2(\bar{x})(e^{-\bar{t}} - 1)}{\cosh(\bar{x}) - \cos(\bar{x})} \\ \rho_{arg} &= \cos(\bar{z}) - \frac{\sin^2(\bar{z})(1 - e^{\bar{t}})}{\cosh(\bar{x}) - \cos(\bar{z})} \\ \rho_s &= \sqrt{1 - \rho_{arg}^2} \\ \xi_s &= \sqrt{\xi_{arg}^2 - 1}. \end{aligned}$$

REFERENCES

- [BM87] A. F. Blumberg and G. L. Mellor. A description of a three-dimensional coastal circulation model. In N. Heaps, editor, *Three Dimensional Coastal Ocean Models*, pages 1–16. Amer. Geophys. Union, 1987.
- [CRB10] B. Cushman-Roisin and J.-M. Beckers. *Introduction to Geophysical Fluid Dynamics: Physical and Numerical Aspects*. Academic Press, 2010.
- [CSA05] P. F. Choboter, R. M. Samelson, and J. S. Allen. A New Solution of a Nonlinear Model of Upwelling. *J. Phys. Oceanogr.*, 35:532–544, 2005.
- [Gil82] A. Gill. *Atmosphere - Ocean Dynamics*. Academic Press, 1982.
- [LC04] S. J. Lentz and D. C. Chapman. The importance of non-linear cross-shelf momentum flux during wind-driven coastal upwelling. *J. Phys. Oceanogr.*, 34:2444–2457, 2004.
- [Ped78] J. Pedlosky. A Nonlinear Model of the Onset of Upwelling. *J. Phys. Oceanogr.*, 8:178–187, 1978.